Received: 3 March 2020 | Revised: 21 December 2020 | Accepted: 4 January 2021

IET Wireless Sensor Systems

DOI: 10.1049/wss2.12019

ORIGINAL RESEARCH PAPER

Design and optimization of printed spiral coils for wireless passive sensors

Babak Noroozi | **Bashir I. Morshed**

Department of Electrical and Computer Engineering, University of Memphis, Memphis, Tennessee, USA

Correspondence

BabakNoroozi, Department of Electrical and Computer Engineering, The University of Memphis, Memphis, Tennessee, USA.
Email: bnoroozi@memphis.edu

Funding information

National Science Foundation, Grant/Award Number: 1637250

Abstract

Monitoring physiological signals during regular life might provide many benefits including early detection of abnormalities and tracking the severities of diseases. A wireless connection between the passive sensor and the scanner eliminates the obtrusive wires, resolves battery-related issues, and makes it easy-to-use. We have previously proposed a wireless resistive analogue passive sensor technique that operates with the help of inductive coupling. The variation of resistive physiological transducer (secondary side) leads to amplitude modulation on the scanner coil (primary side). The design of printed spiral coil (PSC) on printed circuit board, significantly affects the performance of the overall system in terms of sensitivity, the output voltage change as a reflection of the transducer change. To optimize the PSC's profile and maximize the sensitivity, we employ three methods: iterative, analytical, and genetic algorithm (GA). The GA optimized PSCs, as the best result, have been fabricated and the measurement showed a sensitivity of 0.72 m℧ which has 5% (8.8%) deviation from the simulation (theoretical) results. This method can be utilized to design a PSC pair in near-field applications to transfer amplitude modulation with various sizes and fabrication constraints.

1 | INTRODUCTION

Wearables can provide continuous long-term monitoring of physiological parameters. It allows the detection of abnormality and the variation of symptoms severity at the natural life setting instead of confined clinical setup. This is feasible due to advancements that produce lightweight and low-power wearable medical devices and sensors. Fully passive (battery-less) sensors are a promising technology for this case. The optimization of a fully passive wireless sensor is essential, which is addressed here as a progress of our previous research [1].

Bluetooth and WiFi are two common wireless techniques that have been dominantly used in the medical wearable sensors researches and applications [2,3]. The battery requirement, power consumption, hardware complexity, and cost are the major barriers of these active wireless sensors that led to exclude these methods from the scope of this study. With regard to fully passive sensors, radio frequency identifier (RFID) as another wireless technique is also utilized in the wearable system researches and applications [4]. The active chip on the RFID tag requires a power source that is supplied by a wireless signal, an embedded battery, or power harvesting. Such existing passive technologies can share the findings from this study.

We have previously reported [1] a novel wireless resistive analogue passive (WRAP) sensor that a pair of planar spiral coils (PSCs) provide an inductive coupling (magnetic connection) at 13.56 MHz between the scanner (reader) and the sensor. In this approach, the variation of a resistive transducer causes the variation of inducting coupling (Q) to the scanner (primary side). The overall system performance is measured by sensitivity of the link, i.e., the primary voltage changes in response to the transducer variations. A wireless capacitive analogue passive (WCAP) transducer that responds to the body signal employs the same idea of magnetic inductive connection between a fully passive sensor and a scanner circuit [5]. The transducer variation in response to the bio-signal modulates the resonance frequency of the LC resonator on the sensor side. In WCAP method, the transducer capacitance range affects the coil self-inductance optimization, and as a result, the coil design, overall sensitivity, and resonance frequency cannot be independently designed. On the other hand, in

This is an open access article under the terms of the Creative Commons Attribution License, which permits use, distribution and reproduction in any medium, provided the original work is properly cited.

© 2021 The Authors. *IET Wireless Sensor Systems* published by John Wiley & Sons Ltd on behalf of The Institution of Engineering and Technology.

the WRAP [1], the coil characteristics can be optimized for desired resonance frequency and maximum sensitivity independently from the transducer. In addition, a WCAP is more vulnerable to the capacitance disturbances due to body vicinity that affects the probed signal and declines the signal-to-noise ratio (SNR) [6]. Moreover, the WCAP frequency modulation (FM) technique requires a larger bandwidth and complex FM demodulator in the scanner compared to WRAP. Furthermore, the availability of capacitive transducers for different physical signals limits their application further. Towe [7] and Schwerdt [8] reported probing bio-potentials by a varactor transducer through the radio frequency backscattered signal. The major drawback associated with this method in addition to the discussed concerns, is their limited application to the bio-potentials.

In contrast, WRAP sensor method uses resistive variations for both physical signals and bio-potentials, with the help of a resistive transducer or a transadmittance (e.g. MOSFET) device, respectively [9]. Here we attempt to maximize the sensitivity, namely the primary's modulated amplitude in response to a unit change in the transducer resistance. To maximize the sensitivity, a pair of PSCs are optimized by considering the size and fabrication constraints. To the best of our knowledge, existing literature on the inductive wireless connection mainly focuses on the magnetically coupled resonant wireless power transfer in both industrial and medical fields [10].

Near-field antenna design has been also studied in the RFID and near-field communication (NFC) researches. However, their concern about impedance matching, power transfer, data transmission rate, and metal proximity is addressed by component adjustment, antenna shape, and shielding with no discussion on the antenna detailed design [11]. Previously, the measurement showed that a maximum sensitivity can be achieved even by taking the power transfer efficiency as the objective function [1]. The theoretical result of genetic algorithm (GA) showed a better performance in comparison with the four other deterministic optimization methods sensitivity objective function [12].

In this paper, The optimization results of GA, iterative, and analytical methods are compared, and it is shown that the results can be improved by optimizing the individual components prior to the coil optimization. The GA result showed the highest sensitivity and due to its fast and less complex algorithm, its result has been considered as the optimum PSC pair and has been fabricated in three samples. The experimental sensitivity results show less than 9% and 5% disagreement with analytical and simulation results, respectively.

The remainder of this article is organized as follows. In Sections 2 and 3, the hardware concept, schematic model, and the analytical equations are explained. Section 3 describes the different methods for coil optimization and the results are presented in Sections 4 and 5. Section 6 concludes the article. The susceptibility to the capacitors and coil profile tolerances are discussed in supplementary documents.

2 | THE HARDWARE MODEL AND EQUATIONS

2.1 | Circuit schematic

Figure 1 shows the concept of a WRAP system. It consists of primary and secondary circuits that are also known as scanner and sensor, respectively. The resistive transducer variation in the passive secondary side modulates the primary coil voltage through the magnetic field between a pair of PSCs. A sinusoidal AC supply drives the primary circuit at 13.56 MHz within the industry, scientific, and medical (ISM) frequency band. Here, 'sensitivity' is defined as the normalized primary voltage ($V_{\mathrm{OUT}}/V_{\mathrm{OSC}}$ in Figure 1) change to a unit change of transducer resistance as follows:

$$\text{Sensitivity} = \frac{d(V_{\mathrm{OUT}}/V_{\mathrm{OSC}})}{dR_{\mathrm{Transducer}}}\left(\Omega^{-1}\right) \tag{1}$$

The matching/resonator block in Figure 1 consists of capacitors to tune both primary and secondary resonance frequencies on 13.56 MHz as well as matching the impedance between the primary coil and the AC supply. Figure 2 shows the complete circuit schematic where R_P (R_S), C_P (C_S), and L_P (L_S) are the primary (secondary) PSC equivalent components, C_{tp} (C_{ts}) is the tuning capacitor for primary (secondary) resonator, R_{in} is the AC supply internal resistor, and C_{in} is the matching impedance. This configuration in which the primary and secondary tuning capacitors, C_{tp} and C_{ts} (Figure 2), are in parallel with the primary and secondary coils, is called parallel–parallel (PP). We have shown that PP arrangement as compared with three other possible arrangements (SP, SS, and PS) shows the best performance (highest sensitivity and lowest susceptibility to tolerance) [13]. The sensitivity in Equation (1) depends on the component values and the mutual inductance between the primary and the secondary coils, M, that is defined by the primary and secondary self-inductances (L_P and L_S) and the coupling coefficient in Equation (2).

$$M = k\sqrt{L_P L_S} \tag{2}$$

Coupling coefficient (k) depends on the coil physical relative position, size, physical shape, and environment objects. The coupling factor is assumed as a constant parameter in this study and 0.08 is the best experimental value for the setting of this work. Therefore, the sensitivity becomes just a function of the circuit components, as shown in Figure 2.

2.2 | Equations

There are two groups of equations: the circuit analytical equations and the PSC's physical equations. The analytical equations determine the sensitivity as a function of the electrical components shown in Figure 2. The PSC's physical

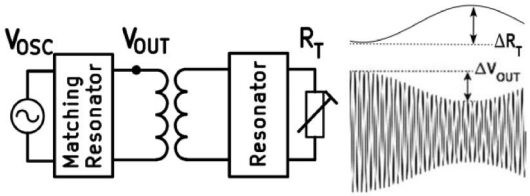

FIGURE 1 (L) The concept of sensitivity and (R) ΔV_{Out} in response to ΔR_T

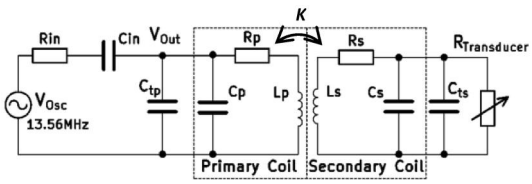

FIGURE 2 Circuit schematic of wireless resistive analogue passive system. C_{tp} and C_{ts} are primary and secondary trimmer capacitors, respectively, and k is the coupling coefficient

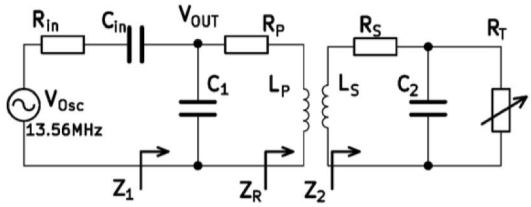

FIGURE 3 Equivalent circuit of the schematic shown in Figure 2. Here: $C_1 = C_{tp}+C_p$ and $C_2 = C_{ts}+C_s$, $V_P = V_{Out}$, and $R_T = R_{Transducer}$

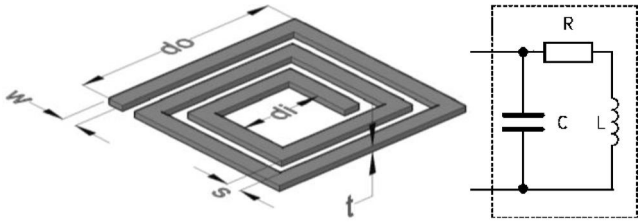

FIGURE 4 (L) Printed spiral coil physical characteristics and (R) the equivalent circuit

equations describe the relation between the PSC equivalent electrical components and its physical profile.

According to Figure 3, the analytical equations are defined in Equations (3)–(8) to calculate the normalized primary voltage (output voltage) derivative versus transducer resistance.

$$Z_2(R_T) = R_S + j\omega L_S + \frac{1}{1/R_T + j\omega C_2} \tag{3}$$

$$Z_R(R_T) = \frac{[M \times \omega]^2}{Z_2(R_T)} = \frac{[k \times \omega]^2 L_P L_S}{Z_2(R_T)} \tag{4}$$

$$Z_1(R_T) = 1 \Big/ \left(j\omega C_1 + \frac{1}{R_P + j\omega L_P + Z_R(R_T)} \right) \tag{5}$$

$$Z_{in} = R_{in} + \frac{1}{j\omega C_{in}} \tag{6}$$

$$\frac{V_{OUT}(R_T)}{V_{in}} = \frac{Z_1(R_T)}{Z_1(R_T) + Z_{in}} \tag{7}$$

$$\text{Sensitivity}(R_T) = \frac{d(V_{OUT}/V_{OSC})}{dR_T} = \frac{d}{dR_T}\left(\frac{Z_1(R_T)}{Z_1(R_T) + Z_{in}}\right) \tag{8}$$

Figure 4 shows the PSC physical characteristics and equivalent circuit. Coil equivalent series resistor is defined in Equations (9)–(12) [14].

$$R = R_{dc} \times \frac{t}{\delta(1 - \exp(-t/\delta))} = \frac{\rho}{W} \times \frac{L_C}{\delta(1 - \exp(-t/\delta))} \tag{9}$$

where t is conductor's thickness and according to the printed circuit board (PCB) fabricator it is 0.96 mm, ρ is conductor's resistivity (1.68×10^{-8} Ω m for copper), w is conductor's width (as shown in Figure 4), n is number of turns in the coil, μ is the magnetic permeability of conductor (1.26×10^{-6} H/m for copper), δ and L_C are the skin depth and conductor length, respectively, and are defined in Equations (10) and (11).

$$\delta = \sqrt{\frac{\rho}{\pi \mu f}} \tag{10}$$

$$L_C = 4nd_O - 3nw - (2n-1)^2(s+w) \tag{11}$$

Two adjacent tracks form a capacitor that is defined in Equation (12) [14]. Its dielectric splits between the board coating (air) and the PCB substrate (FR4) with the relative dielectric constant ε_{rc}=1 and $\varepsilon_{rs} = 4.4$, respectively.

$$C = (\alpha\varepsilon_{rc} + \beta\varepsilon_{rs})\varepsilon_0 \frac{t \times L_G}{S} \tag{12}$$

α and β are the empirical constants, $\alpha = 0.9$, $\beta = 0.1$, L_G is the gap length between two tracks, defined in Equation (13), and s is the space between tracks (Figure 4).

$$L_G = 4(d_O - nw)(n-1) - 4n(n+1)s \tag{13}$$

Since the PSC self-inductance has a critical influence on the sensitivity, the comparison of the calculation results between the different methods: Current Sheet [15], Modified Wheeler [15], Modified Grover [16], and Monomial Fit [16] showed that the Current Sheet has the minimum deviation from the experimental results. Therefore, the Current Sheet with Equation (14) has been adopted for the PSC self-inductance calculation [15].

$$L = \frac{1.27\mu_0(d_O + d_i)n^2}{4}\left[\ln\left(\frac{2.07}{\varphi}\right) + 0.18\varphi + 0.13\varphi^2\right] \tag{14}$$

where μ_0 is the air magnetic permeability and φ is called fill-ratio:

$$\varphi = \frac{d_O - d_i}{d_O + d_i} = \frac{n(s+w) - s}{d_O - n(s+w) + s} \tag{15}$$

If $s < 3w$, the maximum error for Equation (14) is less than 8% [15].

3 | METHODS

The sensitivity in Equation (8) is a multivariable function including PSC physical specifications (Figure 4): number of turns (n), conductor width (w), space between two tracks (s), PSC's outer and inner sizes or diameters (d_O and d_i) for both primary and secondary as well as circuit components: C_{tp}, C_{ts}, and C_{in}. A sensor with 1 KΩ resistance is considered as the target transducer. The objective function in Equation (8) along with Equations (9), (12), and (14) form a complex multivariable function.

By choosing the secondary coil size as small as 20 mm for ease-of-use of the sensors and users' comfort, the variables reduce to 10: d_{O1}, n_1, s_1, w_1, n_2, s_2, w_2, C_{tp}, C_{ts}, C_{in}. The coil's internal size is defined from the conductor's width, the gap between two conductors, number of turns, and the PSC's external size as follows:

$$d_i = d_O - 2nw - 2(n-1)s \tag{16}$$

To make the optimization faster and more accurate, we break the optimization process into two steps. In the first step, the best components including primary/secondary self-inductances and the capacitors are specified. In the second step, the coil profiles which generate the best match to the step 1 self-inductance results are determined.

3.1 | Electrical components optimization

According to Figures 2 and 3, the tuning and the coil intrinsic capacitors form two parallel capacitors in the primary and secondary are denoted as C_1 and C_2. For any L_P and L_S pair, a unique combination of C_1, C_2, and C_{in} can be found to maximize the sensitivity. Table A1 shows the maximum sensitivity and the optimum component for two self-inductance ranges. For each pair of (L_P, L_S) within the range, the circuit components are optimized for the maximum sensitivity by employing the GA technique (for more details, see the supplementary documents).

3.2 | Optimization of PSC structure

In the second step, we maximize the sensitivity in Equation (8) for the PSC primary and secondary profiles, (**d_{O1}**, n_1, s_1, w_1, n_2, s_2, w_2) using the results of the first step in Table A1 . Through the first step, the components for all possible (L_P, L_S) pairs within the range, are optimized and the results are utilized in the second step, coil profile optimization. We use three approaches to find the optimum coil's profile: GA, iterative, and analytic. GA as a fast and appropriate method for a multivariable and complex function does not provide any circuitry and (fabrication) tolerances insight. Analytic approach for the circuitry analysis and the iterative approach as the method that we have used before are also utilized for comparison [1]. In all the following methods, the condition in Equation (17) is satisfied to keep both coil's self-inductance and quality factor at the maximum level, simultaneously [17].

$$d_{ij} = d_{Oj} - 2n_j w_j - 2(n_j - 1)s_j \geq 0.5 d_{Oj} \tag{17}$$

where j=1 for primary and j=2 for secondary coil.

3.2.1 | Iterative optimization method

We had adopted an iterative method for coil's profile optimization previously [1], and we use it here with some modifications as shown in Figure 5. In this method, each step maximizes the sensitivity objective function (8) for two variables out of seven within the defined range. The iteration repeats if the objective function growth is good enough or greater than a specified value (known as error).

3.2.2 | Analytical optimization method

Figure 6 shows the flowchart of analytical method. This method gives an analytic insight to the coil design. In the other two optimization methods, the best primary and secondary coil profiles are found without tolerance analysis. However, the analytical method starts with optimum self-inductances in Table A1and finds the coil profiles that generate the optimum self-inductances with minimum susceptibility to the tolerances.

The optimum L_P and L_S in Table A1are not precisely feasible due to the discrete nature of the coil physical elements: n, s, and w. In addition, a PSC with a specific self-inductance does not have a unique profile (d_O, n, s, w). Moreover, the optimum design is the one that has the minimum change due to the fabrication tolerances: $\Delta s = \pm 1\ mil$ and $\Delta w = \pm 0.5\ mil$, according to the PCB fabrication service (Oshpark LLC). Hence, the best profiles are those that make the closest values to the optimized L_P and L_S and show the minimum

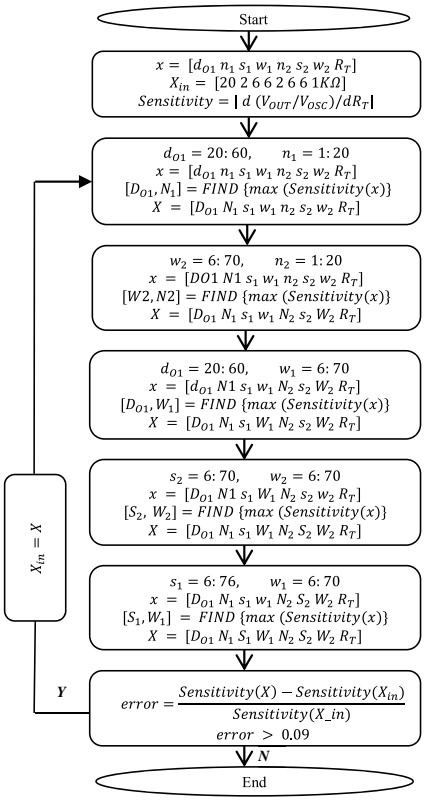

FIGURE 5 Iterative method (d_{O2} = 20 mm). The capital variables represent the optimum values from previous steps and the small variables represent the variables that are being optimized in each step

susceptibility to the fabrication tolerance. According to Figure 6, Steps 2 and 3 indicate excluding the coil profiles whose self-inductances do not meet the minimum error to the target self-inductance. Steps 4 and 5 in Figure 6 rank the effect of fabrication tolerances on the sensitivity and adopt the profiles with the minimum vulnerability to the tolerances.

3.2.3 | GA optimization method

A typical classic optimization algorithm generates a single point and through an iterative deterministic computation tries to approach to the optimum point. In contrast, GA generates a broad random population and by using different methods of mutation, crossover, scaling, and selection, finds the next generation to converge to the optimum point. In addition, GA is fast and appropriate method for a discrete function with no need for straightforward derivative. GA is described with the flowchart in Figure 7. In the coil optimization problem, all the variables are specified as discrete with the lower and upper bounds specified in Table A2 . The nonlinear constraints in Equation (17) define a minimum limit for the primary and secondary internal coil sizes. The important GA setting in the coil optimization problem is shown in Table A3. The parameters are set based on GA average performance over multiple runs with the selected parameters.

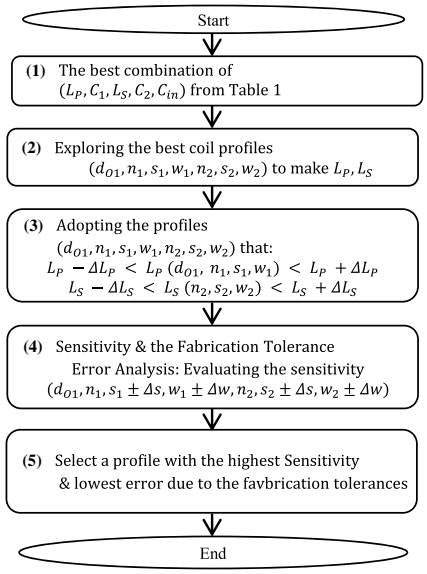

FIGURE 6 Analytical method, flowchart

4 | THEORETICAL RESULTS

This section presents the theoretical results of the optimization methods described in Section 3.2. The optimum capacitors for range (L_P: 3–5 μH and L_S: 3–6 μH) in Table A1 , are applied for the three optimization methods. For all calculations the coupling factor (k), transducer resistance, and the secondary outer size are considered as 0.08, 1 kΩ, and 20 mm, respectively. For the analytical method, due to the discrete nature of the coil parameters, the minimum errors of feasible L_P and L_S comparing to the optimum values in Table A1 are 0.03% and 1.08%, respectively (Step 3 in Figure 6). The possible primary and secondary PSC profiles are shown in Table (A4) . Table shows the optimum sensitivity for all combination of nine primary profiles with one secondary profile in Table A4. According to Table A5 , design 6 shows the highest sensitivity and then, it is considered as the analytical optimum design.

The optimum results and the maximum influence of tolerance are shown in Table A6 for all three methods. The PSC physical specifications affect the coupling factor. However, if we ignore the effect of coil parameters on the coupling factor, the GA results with the highest sensitivity are selected for the rest of this article (Table A6).

5 | FABRICATION, SIMULATION, AND MEASUREMENT RESULTS

5.1 | Measuring the coupling factor (k)

The PCB shown in Figure 8 has been designed with KiCad based on the GA results in Table A6 and was fabricated in three samples. Since the optimization has been performed for k = 0.08, we must adjust the coupling factor on this value before any experimental measurement. Distance between the

primary and secondary coils is the only adjustable parameter to tune the coupling factor.

One way to estimate the coupling factor is measuring the mutual inductance (M) and calculating the coupling factor by using Equation (2). Mutual inductance (M) can be calculated by Equation (18) and measuring the secondary coil open circuit voltage.

$$V_{S-OPEN} = j\omega M I_{Primary} \tag{18}$$

Accessing to the primary current ($I_{Primary}$) and zeroing the secondary current are not feasible due to the primary and secondary coil intrinsic capacitors (C_P and C_S in Figure 2). The effect of intrinsic capacitors on the primary and secondary current decreases by decreasing the working frequency but it also attenuates the secondary voltage which makes it immeasurable due to a poor SNR. Thus, we adopted a practical method for measuring the mutual inductance [18]. In this method, an LCR analyzer (Agilent 4294A, 40 Hz-110 MHz) measures the equivalent self-inductance of aiding and opposing connection of primary and secondary coils and the mutual inductance (M) is calculated by:

$$M = \frac{L_{aid} - L_{opp}}{4} \tag{19}$$

where L_{aid} and L_{opp} are the measured self-inductances in aiding and opposing connection of two coils, respectively. Figure 9 shows the measurements results by using Equation (19) and the measured self-inductances for three pairs of PSCs. As mentioned on Figure 9, all three PSC pairs are in good agreement for $k = 0.08 \pm 0.003$ at 16-mm distance. The result is in complete agreement with the simulation results with FEA tool, COMSOL (COMSOL Inc., Burlington, MA) [19]. To the best knowledge of the authors, there is no single accurate expression in the literature to calculate the coupling factor between two rectangular PSCs. We have used the equation that proposed by Grover [20], generalized by Babic et al. [21], and modified by [22] which have been adopted by some researches [23]. However, the result is not consistent with Figure 9 which is also verified by the circuitry simulation (of secondary voltage). Therefore, according to experimental results, we adjusted the distance between primary and secondary PSCs on 16 mm to obtain $k = 0.08$. Generally, coupling factor of PSCs is smaller than the traditional coils. While k is less than 0.1 at few millimetres distance in PSCs [24], it can reach to tenths at the centimetres distance range in the traditional wired coil [25].

5.2 | Measuring the sensitivity

Since the fabricated PSCs do not show the exact calculated equivalent components (Table A6), we must find the new optimum C_1, C_2, and C_{in} according to the fabricated PSC equivalent circuit. The measurement results show the equivalent coil series resistor does not match with Equation (9). Several reasons can lead to this discrepancy, including fabrication materials (ϱ), w, s, t (conductor thickness) tolerances,

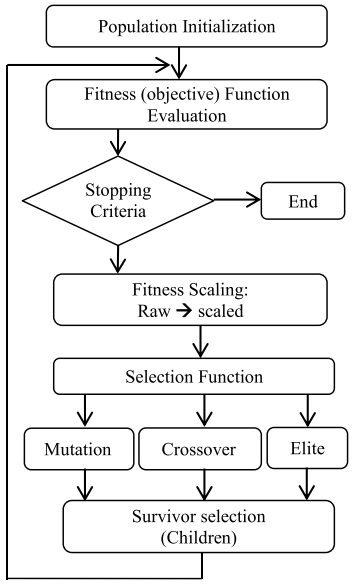

FIGURE 7 Genetic algorithm flowchart

and inaccuracy in Equation (9). However, the optimization theoretical results with measured resistors are in complete agreement with the measured and simulated sensitivity. Table A7 shows the measured components, new optimum capacitors, and the maximum sensitivity by the GA method. The sensitivity decline and the major changes in the optimum capacitors are thoroughly due to the coils' series resistors. Figure 10 shows the experimental setup. The voltage across the primary coil is measured by an oscilloscope (Agilent, Model DSO-X 2024A, Probe Tektronix TPP0200) with the equivalent R_{OSC} = 10 MΩ and C_{OSC} = 11.5 pF. Figure 11 shows the schematic of the circuit under the test. The optimum capacitors (see Table A7) fine-tuned by a series trimmer with signal generator and parallel trimmers with primary and secondary coils. We measured the primary voltage for six transducer resistances from 935 to 1235 Ω and calculated the sensitivity by using Equation (20) and the results are shown in Figure 12.

$$Sensitivity(R_i) = \frac{\Delta V_P}{\Delta R_{Transducer}} = \frac{V_P(R_i) - V_P(R_j)}{R_i - R_j} \tag{20}$$

R_i and R_j are two consecutive resistors out of six resistors. It is worth to mention that the sensitivity in Table A7 is the normalized sensitivity in Equation (8) that shows the primary voltage change due to 1 Ω transducer change for 1 V input voltage (V_{OSC}). Thus, according to Figure 11 with 10 V input voltage, the sensitivity in Table A7 is comparable with Figure 12 by considering a factor of 10.

5.3 | Simulation and theoretical results

The sensitivity is measured by varying the transducer resistance around its nominal value, that is, 1 KΩ, and substitute its

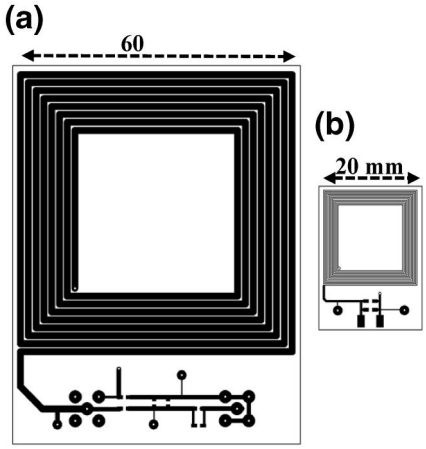

FIGURE 8 The PCB design based on GA results: (a) primary and (b) secondary

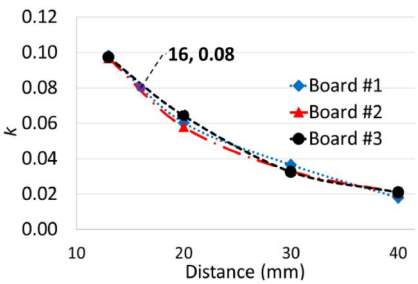

FIGURE 9 Measuring the coupling factor for three fabricated printed spiral coils using Equation (21). For $D = 16$ mm, coupling factor is 0.08 ±0.003 for three boards

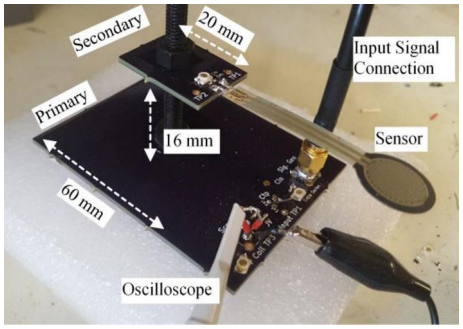

FIGURE 10 Experimental setup for sensitivity measurement

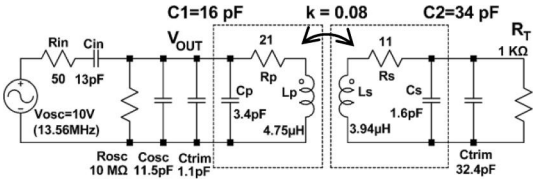

FIGURE 11 The schematic for the circuit under the test. Printed spiral coil shows the equivalent components for Board 1

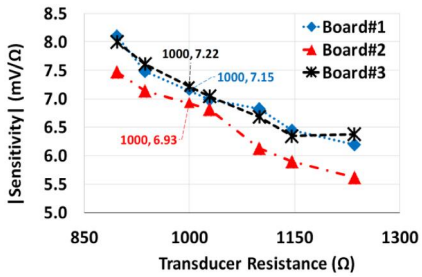

FIGURE 12 Average measured sensitivity for three fabricated boards. The sensitivity for $R_T = 1$ kΩ is 7.5, 6.9, and 7.2 for Board 1 to Board 3, respectively

associate voltage in Equation (20). The final circuit shown in Figure 11, has been used for simulation, measurement, and theoretical calculation. LTspice (Linear Technology, Milpitas, CA) was employed to simulate the voltage change in response to the transducer resistance variation. A MATALB code developed to compute Equations (2)–(8) as the theoretical sensitivity for different transducer resistances. According to Table A7, the expected sensitivity for 1 KΩ transducer resistance, is 7.9 m℧ (the average sensitivity for three fabricated boards) which is in good match with simulation and measurement values. Figure 13 shows the average results of measurement, simulation, and theoretical for three PSC pairs. As this figure shows, the simulation, calculation, and measurement results are in good agreement with the maximum 8.8% difference between the calculation and measurement at $R_S = 1$ kΩ. According to Figure 11, the sensitivity has the descending trend which is reasonable.

6 | DISCUSSION AND CONCLUSION

Previously, we had designed an optimum PSC pair to maximize the sensitivity by adopting and applying an iterative method for maximum power transfer. First we defined the sensitivity as a function of circuit components and the coil profiles. Then we used two more methods, GA and analytical, in addition to the iterative method, to find the optimum coil profiles at 1 kΩ transducer resistance. For coil profile optimization, we first found the best impedance matching (C_{in}) and tuning capacitors (C_1 and C_2) for the defined self-inductance ranges. Although the maximum sensitivity resulted from all three methods are in the same range, since the GA is faster, more reliable, easier to apply, and has the highest sensitivity, its result was adopted for fabrication. As the fabricated PSCs do not show the exact designed self-inductance, the new components were reoptimized according to the fabricated PSCs. The sensitivity for three sample boards was measured and compared with the theoretical and simulation results. The average measurement result for three boards showed a 0.72 m℧ sensitivity (i.e., 0.72 mV primary voltage change per 1 V of input voltage (V_{OSC}) for 1 Ω change in transducer resistance). The experimental results show 5% and 8.8%

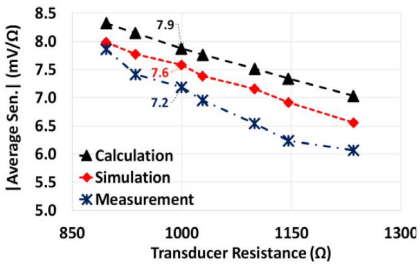

FIGURE 13 The average results for three boards: measurement, simulation, and calculation

difference with the simulation and theoretical results, respectively. More discussion on coil self-inductance range and the susceptibility to the components' tolerances is provided in the supplementary document. In this study, the coupling factor has been taken as a constant value, independent of coil profiles, whereas it is affected by the PSC physical characteristics. The effect of coil profiles on the coupling factor should be introduced in the optimization process that requires further study. In addition, to design a practical wearable sensor based on the optimized PSC pair, the effect of the primary and secondary movements (misalignment) that affects the coupling factor should be also considered in the PSC design. The effects of coil profiles and coil misalignment on the coupling factor are two parameters that should be studied in the coil design and optimization process in future work.

ACKNOWLEDGEMENT

This material is based on work supported by the National Science Foundation under Grant No. 1637250.

REFERENCES

1. Noroozi, B., Morshed, B.I.: PSC optimization of 13.56-MHz resistive wireless analog passive sensors. IEEE Trans. Microw. Theory Techn. 65 (9), 3548–3555 (2017)
2. Lee, B.G., Lee, S.M.: Smart wearable hand device for sign language interpretation system with sensors fusion. IEEE Sensor. J. 8(3), 1224–1232 (2018)
3. Tan, B., et al.: Exploiting WiFi channel state information for residential healthcare informatics. IEEE Commun. Mag. 56(5), 130–137 (2018)
4. Lemey, S., et al.: Wearable flexible lightweight modular RFID tag with integrated energy harvester. IEEE Trans. Microw. Theory Techn. 64(7), 2304–2314 (2016)
5. Salpavaara, T., et al.: Wireless interrogation techniques for sensors utilizing inductively coupled resonance circuits. Proc. Eng. 5, 216–219 (2010)
6. Riistama, J., et al.: Totally passive wireless biopotential measurement sensor by utilizing inductively coupled resonance circuits. Sens. Actuator. 157, 313–321 (2010)
7. Towe, B.C.: Passive backscatter biotelemetry for neural interfacing. In: Proceedings of IEEE/EMBS Conference Neural Engineering, Kohala Coast, HI, USA, pp. 144–147 (2007)
8. Schwerdt, H.N., Chae, J., Miranda, F.A.: Wireless performance of a fully passive neurorecording microsystem embedded in dispersive human head phantom. In: Proceedings of IEEE Antennas Propagation Soc. Int. Symp., Chicago, IL, USA, pp. 1–2 (2012)
9. Consul-Pacareu, S., Arellano, D., Morshed, B.I.: Body-worn fully-passive wireless analog sensors for biopotential measurement through load modulation. In: 2015 IEEE Topical Conference on Biomedical Wireless Technologies, Networks, and Sensing Systems (BioWireleSS), San Diego, CA2015, pp. 1–3
10. Jow, U., Ghovanloo, M.: Design and optimization of printed spiral coils for efficient transcutaneous inductive power transmission. IEEE Trans. Biomed. Circuit Syst. 1(3), 193–202 (2007)
11. Liu, F., et al.: Modeling and optimization of magnetically coupled resonant wireless power transfer system with varying spatial scales. IEEE Trans. Power Electron. 32(4), 3240–3250 (2017)
12. Zhu, J., et al.: NFC antenna with nonuniform meandering line and partial coverage ferrite sheet for metal cover Smartphone applications. IEEE Trans. Antenna. Propag. 65(6), 2827–2835 (2017)
13. Noroozi, B., Morshed, B.I.: Sensitivity optimization of printed spiral coil for wireless resistive analog passive (WRAP) sensors using genetic algorithm. In: 2018 40th Annual International Conference of the IEEE Engineering in Medicine and Biology Society (EMBC), Honolulu, HI, pp. 4653–4656 (2018)
14. Noroozi, B., Morshed, B. I.: The effect of resonator configurations on the optimized sensitivity in the wireless resistive analog passive (WRAP) sensors. 19th Annual IEEE international conference on Inf. Tech. (EITt2019), Brookings, South Dakota, USA, May 20–22 (2019)
15. Mohan, S.S., et al.: Simple accurate expressions for planar spiral inductances. IEEE J. Solid-State Circuit. 34(10), 1419–1424 (1999)
16. Greenhouse, H.: Design of planar rectangular microelectronic inductors. IEEE Trans. Part. Hybrid. Packag. 10(2), 101–109 (1974)
17. Su, Y., et al.: On the relationship of quality factor and hollow winding structure of coreless printed spiral winding (CPSW) inductor. IEEE Trans. Power Electron. 27(6), 3050–3056 (2012)
18. Hesterman, B.: Analysis and Modeling of Magnetic Coupling. Discovery Learning Center, University Of Colorado, Boulder, CO (2007)
19. Noroozi, B., Morshed, B.I.: Coil distance and angle misalignment effects on the mutual inductance for 13.56 MHz WRAP sensors. In: 2018 United States National Committee of URSI National Radio Science Meeting (USNC-URSINRSM), Boulder, CO, pp. 1–2 (2018)
20. Rose, E.B., Grover, F.W.: Formulas and tables for the calculation of mutual inductance and self-inductance. Sci. Paper. Bur. Stand. ((169) (1916)
21. Babic, S., et al.: Mutual inductance calculation between circular filaments arbitrarily positioned in space: alternative to Grover's Formula. IEEE Trans. Magnet. 46(9), 3591–3600 (2010)
22. Raju, S., et al.: Modelling of mutual coupling between planar inductors in wireless power applications. IEEE Trans. Power Electron. 29(1), 481–490 (2014)
23. Yi, Z., et al.: High-efficiency mid-range inductive power transfer employing alternative-winding coils. IEEE Trans. Power Electron. 34(7), 6706–6721 (2019)
24. Wang, F., et al.: A novel intracranial pressure readout circuit for passive wireless LC Sensor. IEEE Trans. Biomed. Circuit. Syst. 11(5), 1123–1132 (2017)
25. Gilabert-Palmer, D., et al.: Measuring coupling coefficient of windings with dissimilar turns' number or tight coupling using resonance. IEEE Trans. Power Electron. 33(11), 9790–9802 (2018)

SUPPORTING INFORMATION

Additional supporting information may be found online in the Supporting Information section at the end of this article.

How to cite this article: Noroozi B, Morshed BI. Design and optimization of printed spiral coils for wireless passive sensors. *IET Wirel. Sens. Syst.* 2021;1–10. https://doi.org/10.1049/wss2.12019

APPENDIX

TABLE (A1) Maximum sensitivity and optimum capacitors for two ranges of primary and secondary self-inductances ($R_P = 1.1\ \Omega$, $R_S = 5\Omega$, $R_T = 1\ K\Omega$, $k = 0.08$)

Range		Result					
L_P (μH)	L_S (μH)	Sensitivity (m℧)	L_P (μH)	L_S (μH)	C_1 (pF)	C_2 (pF)	C_{in} (pF)
3–5	3--6	7	4.91	4.06	24	14	4
8–10	3–6	14	9.85	5.56	12	1	2

TABLE (A2) The lower/upper bounds in GA (d in mm, s and w in mil)

Bound	d_{O1}	n_1	S_1	W_1	n_2	S_2	W_2
Lower	20	2	6	6	2	6	6
Upper	60	20	70	70	20	70	70

TABLE A3 GA option settings

Population initialization	Size	3000
Stopping criteria	Max stall generation	50
	Max St. Time	Inf.
	Max. gen.	200
Fitness scaling		Rank
Selection Function		Stochastic uniform
Mutation	Function	Adaptive feasible
Crossover	Fraction	0.3
	Function	Scattered
Elite	Elite Count	150 (5% Pop.)

TABLE A4 Feasible primary and secondary PSC profiles for Table A1 and (17). The minimum error for L_P and L_S to the target values are 0.03% and 1.08%, respectively.

	Design No.	d_O (mm)	n	d_i (mm)	S (mil)	W (mil)	R (Ω)	C (pF)	L (Actual)(μH)
Primary	1	30	11	18	10	13	1.44	1.64	4.909
	2	40	10	22	7	30	1.76	2.76	4.909
	3	40	8	30	9	16	3.00	1.90	4.910
	4	40	9	26	9	23	2.20	2.03	4.910
	5	40	10	22	17	21	2.50	1.11	4.910
	6	50	9	27	8	44	1.34	2.68	4.910
	7	50	9	27	17	36	1.64	1.24	4.910
	8	60	6	50	8	27	2.08	2.41	4.910
	9	60	6	50	14	22	2.55	1.36	4.910
Secondary	-	20	13	10	7	8	4.22	1.79	4.017

Note. The appendix provides more information from our analysis for interested readers.

TABLE A5 The analytical resultant sensitivity optimization for the PSC primary and secondary profiles in Table A4. Each design shows the feasible L_P and L_S with minimum error to the optimum values in Table A1

Design number	d_{O1} (mm)	d_{i1} (mm)	n_1	S_1 (mil)	W_1 (mil)	R_P (Ω)	C_P (pF)	L_P (μH)	d_{i2} (mm)	n_2	S_2 (mil)	W_2 (mil)	R_S (Ω)	C_S (pF)	L_S (μH)	Sen. (m℧)
1	30	18	11	10	13	3.44	1.64	4.91	10	13	7	8	4.23	1.79	4.02	2.80
2	40	22	10	7	30	1.76	2.76	4.91	10	13	7	8	4.23	1.79	4.02	5.15
3	40	30	8	9	16	3.00	1.90	4.91	10	13	7	8	4.23	1.79	4.02	3.24
4	40	26	9	9	23	2.20	2.04	4.91	10	13	7	8	4.23	1.79	4.02	4.31
5	40	22	10	17	21	2.51	1.11	4.91	10	13	7	8	4.23	1.79	4.02	3.84
6	50	27	9	8	44	1.34	2.68	4.91	10	13	7	8	4.23	1.79	4.02	6.19
7	50	27	9	17	36	1.64	1.24	4.91	10	13	7	8	4.23	1.79	4.02	5.42
8	60	50	6	8	27	2.08	2.41	4.91	10	13	7	8	4.23	1.79	4.02	4.52
9	60	50	6	14	22	2.55	1.36	4.91	10	13	7	8	4.23	1.79	4.02	3.78

TABLE A6 Optimization results for three methods and the effect of fabrication tolerances on the sensitivity

			d_{O1} (mm)	d_{i1} (mm)	n_1	S_1 (mil)	W_1 (mil)	d_{i2} (mm)	n_2	S_2 (mil)	W_2 (mil)	R_P (Ω)	C_P (pF)	L_P (μH)	R_S (Ω)	C_S (pF)	L_S (μH)	Sen. (m℧)
Iterative	Optimum		39	21.5	10	6	29	10.4	15	6	7	1.77	3.177	4.91	5.52	2.44	5.32	5.18
	Tolerance effect	Max. Sen.	39	21.5	10	6	29	10.0	15	6	7.5	1.79	3.177	4.91	5.13	2.41	5.13	5.20
		Min. Sen	39	22.2	10	5	28.5	9.3	15	7	7.5	1.84	3.87	5.09	5.00	2.01	4.78	0.22
Analytical	Optimum		50	26.6	9	8	44	10.4	13	7	8	1.34	2.68	4.91	4.22	1.79	4.02	6.19
	Tolerance effect	Max. Sen.	50	26.6	9	8	44	11.1	13	6	8	1.34	2.68	4.91	4.31	2.14	4.26	6.24
		Min. Sen	50	27.3	9	7	43.5	9.5	13	8	8.5	1.37	3.1	5.03	3.85	1.51	3.67	0.34
GA	Optimum		60	33.6	8	8	58	13.6	11	6	6	1.10	2.87	4.91	5.21	1.93	3.93	6.88
	Tolerance effect	Max. Sen.	60	33.6	8	8	58	13.8	11	5	6.5	1.11	2.87	4.91	4.88	2.35	4.03	6.91
		Min. Sen	60	34.1	8	7	57.5	12.8	11	7	6.5	1.12	3.31	5.00	4.74	1.61	3.63	0.46

TABLE A7 The GA update optimization results for fabricated PSCs

	Measured				(GA) Optimization results			
Board #	L_P (μH)	R_P (Ω)	L_S (μH)-	R_S (Ω)	C_1 (pF)	C_2 (pF)	C_{in} (pF)	$\lvert Sen. \rvert$ (m℧)
1	4.75	21	3.94	11	16	34	13	0.79
2	4.77	21.5	3.98	11.5	16	34	13	0.77
3	4.79	21	3.99	11	16	34	13	0.8

Abbreviations: GA, genetic algorithm, PSC, printed spiral coil.